

Paris W. Barnes,<sup>‡</sup> Michael W.  
Lufaso<sup>§</sup> and Patrick M.  
Woodward\*

Department of Chemistry, The Ohio State  
University, Columbus, OH 43210, USA

<sup>‡</sup> Current address: Materials Science Division,  
Argonne National Laboratory, Argonne, IL  
60439, USA.

<sup>§</sup> Current address: Department of Chemistry  
and Biochemistry, University of South Carolina,  
631 Sumter Street, Columbia, SC 29208, USA.

Correspondence e-mail:  
woodward@chemistry.ohio-state.edu

# Structure determination of $A_2M^{3+}TaO_6$ and $A_2M^{3+}NbO_6$ ordered perovskites: octahedral tilting and pseudosymmetry

Received 10 June 2005  
Accepted 19 January 2006

The room-temperature crystal structures of six  $A_2M^{3+}M^{5+}O_6$  ordered perovskites have been determined from neutron and X-ray powder diffraction data.  $Ba_2YNbO_6$  adopts the aristotype high-symmetry cubic structure (space group  $Fm\bar{3}m$ ,  $Z = 4$ ). The symmetries of the remaining five compounds were lowered by octahedral tilting distortions. Out-of-phase rotations of the octahedra about the  $c$  axis were observed in  $Sr_2CrTaO_6$  and  $Sr_2GaTaO_6$ , which lowers the symmetry to tetragonal (space group =  $I4/m$ ,  $Z = 2$ , Glazer tilt system =  $a^0a^0c^-$ ). Octahedral tilting analogous to that seen in  $GdFeO_3$  occurs in  $Sr_2ScNbO_6$ ,  $Ca_2AlNbO_6$  and  $Ca_2CrTaO_6$ , which lowers the symmetry to monoclinic (space group  $P2_1/n$ ,  $Z = 2$ , Glazer tilt system =  $a^-a^-c^+$ ). The  $Sr_2MTaO_6$  ( $M = Cr, Ga, Sc$ ) compounds have unit-cell dimensions that are highly pseudocubic.  $Ca_2AlNbO_6$  and  $Ca_2CrTaO_6$  have unit-cell dimensions that are strongly pseudo-orthorhombic. This high degree of pseudosymmetry complicates the space-group assignment and structure determination. The space-group symmetries, unit-cell dimensions and cation ordering characteristics of an additional 13 compositions, as determined from X-ray powder diffraction data, are also reported. An analysis of the crystal structures of 32  $A_2MTaO_6$  and  $A_2MNbO_6$  perovskites shows that in general the octahedral tilt system strongly correlates with the tolerance factor.

## 1. Introduction

Since the discovery of  $BaTiO_3$  during World War II, perovskites have been studied extensively for their interesting and important physical properties. Perovskites are known to exhibit ferroelectricity and piezoelectricity ( $BaTiO_3$ ,  $PbTiO_3$ ,  $PbZr_{1-x}Ti_xO_3$ ), non-linear optical behavior ( $KNbO_3$ ), superconductivity ( $Ba_{1-x}K_xBiO_3$  and  $BaBi_{1-x}Pb_xO_3$ ), colossal magnetoresistance ( $La_{1-x}Ca_xMnO_3$ ) and ionic conductivity ( $LaMnO_{3-\delta}$  and  $BaCe_{1-x}Nd_xO_3$ ). Perovskites with an ordered cation arrangement also exhibit interesting physical properties. Examples include  $Sr_2FeMoO_6$ , which exhibits half-metallic conductivity (Sleight & Weiher, 1972; Kobayashi *et al.*, 1998), and  $Ba_3ZnTa_2O_9$ , which is used in mobile telecommunication base stations due to its dielectric properties (Bieringer *et al.*, 2003; Vanderah, 2002).

Octahedral-site cation ordering is particularly favorable when the stoichiometry is  $A_2MM'X_6$  and there is a large difference in oxidation state and/or ionic radii of the  $M$  and  $M'$  cations. Under these circumstances a rock salt-type arrangement of the  $M$  and  $M'$  cations is normally observed, as shown in Fig. 1. While this is far and away the most common type of ordering seen in perovskites, there are other types of ordering, including 2:1 and 3:1 ordering of the octahedral site cations, as

well as layered ordering of the octahedral site and/or the *A*-site cations. The interested reader is referred to works by Anderson *et al.* (1993), Davies (1999) and Mitchell (2002) for more details on cation ordering in perovskites.

Rock-salt (1:1) ordering of the octahedral-site cations doubles the unit cell of the simple undistorted  $AMX_3$  perovskite, changing the space-group symmetry from  $Pm\bar{3}m$  to  $Fm\bar{3}m$ . Both ternary and ordered perovskites are prone to a variety of distortion mechanisms that lower the symmetry of the cubic aristotype structure. The most common type of distortion involves cooperative tilts of the octahedra. Octahedral tilting distortions lead to significant changes in the coordination environment of the *A*-site cation as well as the anion, while retaining the corner-sharing connectivity of the octahedral framework and the local coordination environment of the octahedral-site cation. Notations to describe the various types of octahedral tilting distortions (octahedral tilt systems) have been developed by Glazer (1972) and Aleksandrov (1976). The notation of Glazer will be used throughout this paper.

Several previous analyses report the space-group symmetries and unit-cell dimensions that result from the combination of octahedral tilting and octahedral-site cation ordering (Alexandrov & Misyul, 1981; Woodward, 1997*a*; Bock & Müller, 2002). The most recent and probably the most accurate of these works is a group-theoretical analysis (Howard *et al.*, 2003), which also contains a discussion on how to recognize the presence and type of octahedral tilting distortion from the analysis of reflection splitting and systematic absences. In some cases, the pseudosymmetry is sufficiently high that analysis of reflection splitting can be misleading, because the true crystallographic space-group symmetry is lower than the symmetry suggested by the unit-cell dimensions. Such cases

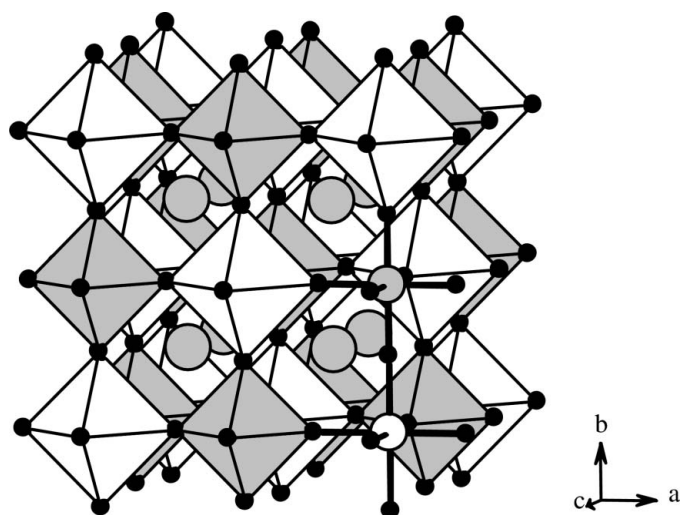


**Figure 1**  
Conventional view of the cubic aristotype (space group  $Fm\bar{3}m$ ) double perovskite structure showing corner-sharing  $MX_6$  and  $M'X_6$  octahedra with the *A* cations residing in the cavities formed by the octahedral network. Legend:  $[MX_6]$ : white octahedral/sphere;  $[M'X_6]$ : grey octahedral/sphere; *A*: cross-hatched spheres; *X*: filled spheres.

represent special challenges for the crystallographer attempting to determine their structures from powder diffraction data. This is the case for five of the six compounds whose structures are reported in this paper.

## 2. Experimental

### 2.1. Synthetic methods

$Sr_2CrTaO_6$ ,  $Ca_2CrTaO_6$  and  $Ca_2AlNbO_6$  were made *via* conventional solid-state techniques using stoichiometric amounts of high-purity  $SrCO_3$ ,  $Cr_2O_3$ ,  $Al_2O_3$  and  $Ta_2O_5$ .  $Sr_2ScNbO_6$  was synthesized by a similar approach from stoichiometric amounts of  $SrCO_3$  and  $ScNbO_4$ , while  $Ba_2YNbO_6$  was prepared from  $BaCO_3$  and  $YNbO_4$ . While these latter two compounds will also form from the direct reaction of  $SrCO_3$  ( $BaCO_3$ ),  $Sc_2O_3$  ( $Y_2O_3$ ) and  $Nb_2O_5$ , it is difficult to obtain single-phase samples through direct reaction owing to the sluggish reactivity of  $Sc_2O_3$  ( $Y_2O_3$ ). All reactions were carried out in alumina crucibles. In all cases multiple heating and grinding cycles were completed before single-phase products were observed or the level of impurity became negligibly small and unchanged by further heat treatments. The final annealing temperatures were in the range 1523–1773 K.

$Sr_2GaTaO_6$  was prepared in a  $SrCl_2$  flux, which was followed by annealing treatments at higher temperature. This method has been described previously for the synthesis of  $Sr_2AlTaO_6$  and  $Sr_2AlNbO_6$  (Woodward *et al.*, 1994). Stoichiometric amounts of high-purity  $SrCO_3$ ,  $Ga_2O_3$  and  $Ta_2O_5$  were mixed and preheated in an alumina crucible. Next, a twofold excess (by mass) of dry  $SrCl_2$  (melting point = 1146 K) was added to the reaction mixture. The mixed powders were placed in a platinum crucible and heated at 1173 K for 12 h. The desired product was obtained by dissolving the  $SrCl_2$  flux in dilute ( $\sim 1M$ ) nitric acid and separating it from the solution by filtration. The sample was then annealed at 1773 K to increase the extent of octahedral-site cation ordering.

### 2.2. Powder diffraction data collection

Laboratory X-ray powder diffraction (XRPD) data were collected on a Bruker Advance D8 diffractometer equipped with an incident-beam Ge monochromator and a position-sensitive detector. Data were collected from 15 to  $120^\circ 2\theta$  with a step size of  $\sim 0.0144^\circ$  (2 s per step) using  $Cu K\alpha_1$  radiation. The presence of barium in  $Ba_2YNbO_6$  produced fluorescence that was problematic for the position-sensitive detector (PSD). Therefore, an XRPD pattern for this compound was collected on a Rigaku Geigerflex diffractometer. This diffraction pattern was collected from 15 to  $120^\circ 2\theta$  with a  $0.04^\circ$  step size at 2.5 s intervals using a  $Cu$  radiation source.  $Cu K\alpha_1$  ( $\lambda = 1.54056 \text{ \AA}$ ),  $K\alpha_2$  ( $\lambda = 1.54439 \text{ \AA}$ ) and  $K\beta$  ( $\lambda = 1.392218 \text{ \AA}$ ) radiation were all present in the diffraction data and were appropriately handled in the Rietveld refinements. The intensity of the  $K\beta$  radiation was significantly reduced by using a nickel-foil filter placed before the receiving slit. The divergence, receiving and scatter slits used were 1.0, 0.6 and  $1.0^\circ$  in width, respectively.

Synchrotron X-ray powder diffraction data were collected on the X7A beamline of the National Synchrotron Light Source (NSLS) at Brookhaven National Laboratory (BNL). Monochromatic radiation was obtained by using a Ge(111) channel cut-crystal monochromator in the incident beam. The sample was loaded into 0.2–0.3 mm diameter thin-walled capillaries, which were rotated during data collection to minimize the effects of preferred orientation and/or texture. The diffracted radiation was detected using a linear multiwire PSD.

Neutron powder diffraction (NPD) data were collected using the BT-1 32 detector neutron powder diffractometer at the NIST Center for Neutron Research (NCNR), NBSR. A Cu(311) monochromator with a 90° take-off angle,  $\lambda = 1.5402(2)$  Å, and in-pile collimation of 15' arc were used. Data were collected over the range 3–168°  $2\theta$  with a step size of 0.05° for 4–5 h on 8–10 g samples packed in 50 mm long neutron-transparent vanadium containers with a diameter of 10.8 mm. Further details can be found on the NCNR web site (<http://www.ncnr.nist.gov/>). The neutron diffraction patterns for Sr<sub>2</sub>CrTaO<sub>6</sub> and Ca<sub>2</sub>CrTaO<sub>6</sub> were collected on the high-resolution neutron powder diffractometer at the high-flux beam reactor (HFBR) at Brookhaven National Laboratory (BNL) using a wavelength of 1.8857 Å and a step size of 0.02°  $2\theta$ .

### 2.3. Powder diffraction data analysis

The neutron and synchrotron powder diffraction data were analyzed using the Rietveld method as implemented in the EXP-GUI/GSAS software package (Larson & von Dreele, 2000; Toby, 2001). Reflections were modeled using a type II pseudo-Voigt profile function. Initial atomic positions for the structural refinement were generated for all compositions using the 1:1 *M*-cation ordered option in the perovskite structure prediction software *SPuDS* (<http://www.chemistry.ohio-state.edu/~mlufaso/spuds/>; Lufaso & Woodward, 2001). The extension of *SPuDS* to ordered perovskites is discussed in more detail in the following article (Lufaso *et al.*, 2006). Partial octahedral-site cation ordering was refined under the constraints that (a) the overall stoichiometry remains  $A_2MM'O_6$  and (b) the octahedral sites remain fully occupied. The scale factor, peak-shape parameters, lattice parameters, atomic positional parameters and displacement parameters were all refined during the course of the analysis.

In  $A_2MM'O_6$  perovskites where the *M* and *M'* cations are partially ordered, antiphase boundaries (APBs) in the ordering sequence can and often do occur. The presence of APBs leads to extra broadening of the peaks that arise due to cation ordering (Woodward *et al.*, 1994). This feature could not easily be treated using *GSAS*. Therefore, XRPD data were analyzed using the *WINPLOTR/Fullprof* Rietveld package (Rodríguez-Carvajal, 1993; Roisnel & Rodríguez-Carvajal, 2001). Full refinements were carried out using the atomic positions and lattice parameters obtained from analysis of the NPD data.

As discussed below, both NPD and XRPD data provide useful information regarding the crystal structures of these perovskites. The resolution of the XRPD data is higher, which is useful for analysis of the peak splitting. Furthermore, for the samples analyzed in this study the contrast in the X-ray scattering powers of the *M* and *M'* cations was generally higher than the neutron scattering-length contrast. On the other hand, analysis of the NPD data yields more accurate values of the oxygen positions and displacement parameters, particularly when the pseudosymmetry is high. While there are merits to fitting both types of diffraction data simultaneously with a single structural model, there are also complications to this approach. In this study the aforementioned anisotropic peak broadening that originates from antiphase boundaries cannot easily be dealt with in a combined refinement. Therefore, the NPD and XRPD data have been refined separately. The results of the neutron refinements are presented first, as they give the most accurate atomic coordinates. The cation ordering and unit-cell parameters obtained from the X-ray refinements are presented separately. The X-ray results provide the most accurate assessment of both cation ordering and distortion of the unit cell.

### 2.4. Identification of the tilt system and space group

The diffraction patterns of all perovskites have similar features, even though the symmetries of perovskites can range from triclinic to cubic. Glazer (1972) pointed out that in order to accurately determine the space group of a distorted perovskite from powder diffraction data it is essential to carefully examine the pattern, looking for indications of reflection splitting and the presence of 'extra' reflections. He went on to write that this task '...can be particularly difficult when the splitting of the originally cubic reflections is small and the difference reflections arise from weak scatterers (Glazer, 1975)'. Our understanding of octahedral tilting distortions in perovskites has advanced considerably since Glazer's pioneering studies in the 1970s. Of particular relevance are the studies of Howard and Stokes, who have applied group-theory methods to analyze the effects of octahedral tilting distortions on the space-group symmetries of perovskites (Howard & Stokes, 1998, 2002, 2004, 2005). Darlington (2002) has published a related but independent approach based on the decomposition of vibrational normal modes. Complimentary to these works is the study by Woodward (1997b) which considered crystal chemical implications and relative energies associated with competing types of octahedral tilting. Howard *et al.* (2003) have specifically considered octahedral tilting in rock-salt ordered perovskites and discussed some approaches and possible pitfalls to the structure determination process. The approaches outlined in that paper have been used in this work to correctly determine the structure of six highly pseudosymmetric rock salt ordered perovskites.

To facilitate the discussion contained in the following sections it is instructive to realise that cation ordering, in-phase octahedral tilting and out-of-phase octahedral tilting all

lead to a reduction in translational symmetry, thereby expanding the unit cell. Consequently, these distortions give rise to sets of reflections where the  $h$ ,  $k$  and  $l$  values are related to each other in specific ways. This observation was made 30 years ago by Glazer and falls directly out of the more rigorous treatments of Howard and Stokes, and of Darlington. If the peaks in the diffraction pattern are indexed using a double-edge primitive cubic cell (for oxides,  $a \simeq 8 \text{ \AA}$ ), the Miller indices can be classified into one of four categories:

(i) sublattice reflections (or fundamental perovskite reflections) where  $h$ ,  $k$  and  $l$  are all even numbers.

(ii)  $R$ -point reflections where  $h$ ,  $k$  and  $l$  are all odd numbers. These reflections can arise from either octahedral-site cation ordering or out-of-phase octahedral tilting.

(iii)  $M$ -point reflections where two of the Miller indices are odd numbers and one is an even number. These reflections are an unambiguous sign of in-phase octahedral tilting.

(iv)  $X$ -point reflections where two of the Miller indices are even numbers and one is an odd number. These reflections arise from coupling of the  $R$ -type modes corresponding to out-of-phase octahedral tilting and  $M$ -type modes corresponding to in-phase octahedral tilting.

If we limit the discussion to oxides and fluorides, which account for the majority of perovskites, it is possible to make some quantitative statements about the intensities of the superlattice reflections. The cation ordering contribution to the  $R$ -point reflections is strongly dependent upon the scattering power contrast between octahedral-site cations, which can be quite variable and different for X-rays and neutrons.

When this contribution is large, for example in X-ray diffraction studies of compounds where the  $M$  and  $M'$  cations have very different atomic numbers or in neutron diffraction studies where one of the two ions has a negative scattering length, it can mask the out-of-phase octahedral tilting contribution to the  $R$ -point reflections, thereby complicating the structure determination process. In the absence of observable peak splitting, the subtle distinction between out-of-phase tilting and the absence of tilting lies in the intensities of the  $R$ -point reflections. A relevant point in this regard is the observation that for  $R$ -point reflections where  $h = k = l$  (*i.e.* 111), the contribution due to octahedral tilting is particularly weak. Therefore, significant intensities associated with such peaks can generally be attributed to cation ordering.

The  $X$ -point reflections are typically the weakest of the three classes of superlattice reflections in neutron data sets. This is not necessarily the case in X-ray data because the simultaneous presence of both in-phase and out-of-phase tilting, which gives rise to the  $X$ -point reflections in the first place, also tends to drive displacement of the  $A$ -site cation. Since the  $A$ -site cation typically scatters X-rays more strongly than the anions, this enhances the intensities of the  $X$ -point reflections with respect to the other classes of superlattice reflections, particularly with respect to the  $M$ -point reflections that derive intensity only from octahedral tilts. Whilst it is true that  $A$ -site cation displacements are allowed by symmetry in tilt systems such as  $a^0b^-b^-$  and  $a^-a^-a^-$ , where no in-phase tilting occurs, *SPuDS* modeling shows that  $A$ -site displacements are zero in these tilt systems, provided the octahedra remain perfectly symmetric, and very small in real crystals where octahedral distortions are allowed (Lufaso *et al.*, 2006).

### 3. Results

#### 3.1. $\text{Ba}_2\text{YNbO}_6$

The earliest reports of the synthesis and structure of  $\text{Ba}_2\text{YNbO}_6$  ( $\tau = 0.980$ ) can be found in papers by Brixner (1960) as well as Filip'ev & Fesenko (1961). In both papers the structure is reported as primitive cubic with  $Pm\bar{3}m$  space-group symmetry ( $a \simeq 4.2 \text{ \AA}$ ), implying a disordered Y/Nb distribution. Subsequently,  $\text{Ba}_2\text{YNbO}_6$  has been reported as a cubic ordered double perovskite (Evdokimov & Men'shenina, 1982) and more recently as monoclinic with  $P2_1/n$  space-group symmetry (Henmi *et al.*, 1999). It is difficult to determine the degree of cation ordering from the XRPD data

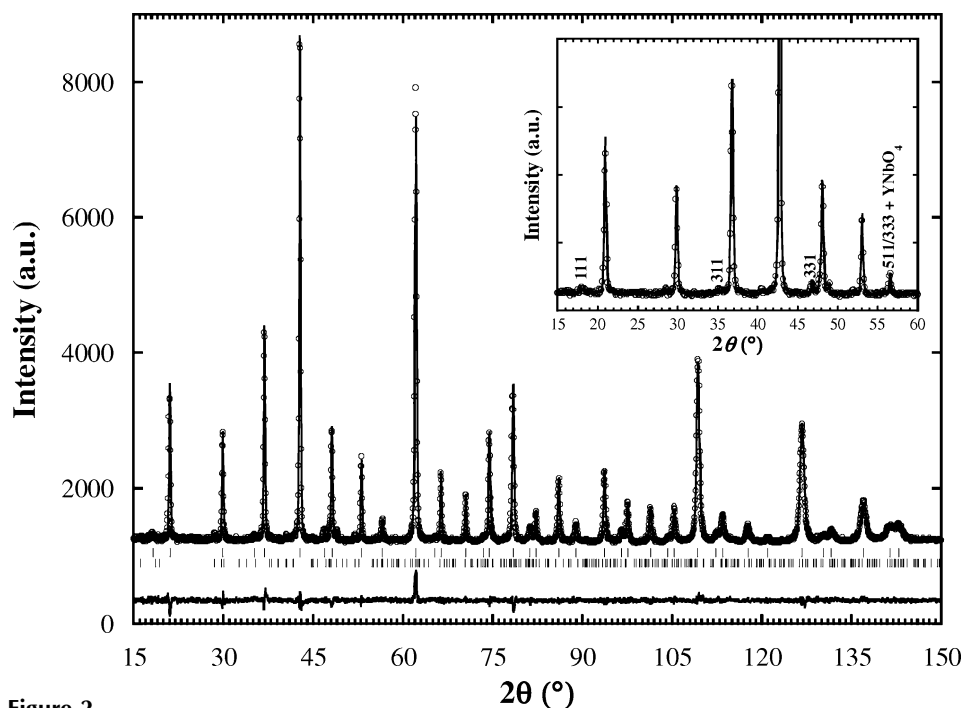


**Figure 2**

Observed neutron diffraction pattern along with calculated and difference patterns from the Rietveld refinement of  $\text{Ba}_2\text{YNbO}_6$ . The upper set of vertical tick marks indicates the expected  $2\theta$  position of the reflections. The lower set of reflection position markers corresponds to a trace of unreacted  $\text{YNbO}_4$ . The inset emphasizes key  $R$ -point reflections that reveal the cation ordering and the oxygen displacement toward niobium.

**Table 1**

The crystal structure of Ba<sub>2</sub>YNbO<sub>6</sub> as determined from neutron powder diffraction data.

The space-group symmetry is *Fm* $\bar{3}$ *m*. The cubic cell edge is  $a = 8.4411(1) \text{ \AA}$ . The goodness-of-fit parameters are  $R_p = 0.039$ ,  $R_{wp} = 0.0449$  and  $\chi^2 = 1.02$ . The refinements showed 3.1 (2)% of unreacted YNbO<sub>4</sub> was present.

Site	<i>x</i>	<i>y</i>	<i>z</i>	$U_{iso} (\text{\AA}^2)$	
Ba	8( <i>c</i> )	1/4	1/4	1/4	0.0091 (2)
Y	4( <i>a</i> )	0	0	0	0.0063 (4)
Nb	4( <i>b</i> )	1/2	0	0	0.0060 (4)
O	24( <i>e</i> )	0.26285 (8)	0	0	†

† Anisotropic atomic displacement parameters were refined for Ba<sub>2</sub>YNbO<sub>6</sub>.  $U^{11} = 0.0077(4) \text{ \AA}^2$ ;  $U^{22} = 0.0222(3) \text{ \AA}^2$ .

because Y<sup>3+</sup> and Nb<sup>5+</sup> are formally isoelectronic. This can easily lead to the incorrect assumption that Y<sup>3+</sup> and Nb<sup>5+</sup> cations are completely disordered. Yet, yttrium(III) and niobium(V) have an oxidation state difference of two and more importantly a large difference in ionic radii (0.260 Å). This combination should stabilize a highly ordered arrangement of yttrium(III) and niobium(V) (Anderson *et al.*, 1993). Close examination of the XRPD data shows evidence of a small peak at *ca* 18.2° 2θ, corresponding to the 111 reflection. This reflection is also seen in the NPD data, as shown in the inset of Fig. 2, where the presence of *R*-point superlattice peaks can clearly be seen. Although there is no indication of reflection splitting, refinements were also carried out using *a*<sup>0</sup>*a*<sup>0</sup>*c*<sup>-</sup> (*I4/m*) and *a*<sup>-</sup>*a*<sup>-</sup>*a*<sup>-</sup> (*R* $\bar{3}$ ) models to test for the presence of out-of-phase tilts. No improvement in the fit was observed upon lowering the symmetry. The goodness-of-fit parameter,  $\chi^2$ , was 1.13 for the *I4/m* structure, 1.27 for the *R* $\bar{3}$  structure and 1.02 for the *Fm* $\bar{3}$ *m* structure. In principle, the  $\chi^2$  value for the tetragonal and rhombohedral structures should be as low

as that obtained for the cubic structure, but in practice this is not always observed. When compared with the  $\chi^2$  differences seen for tetragonal perovskites in the following section these values can be considered nearly equivalent. Thus, we conclude that Ba<sub>2</sub>YNbO<sub>6</sub> adopts the aristotype *Fm* $\bar{3}$ *m* cubic structure at room temperature. The refined crystal structure of Ba<sub>2</sub>YNbO<sub>6</sub> is given in Table 1 and illustrated in Fig. 1. The Rietveld fit to the NPD data is shown in Fig. 2.

### 3.2. Sr<sub>2</sub>GaTaO<sub>6</sub> and Sr<sub>2</sub>CrTaO<sub>6</sub>

Sr<sub>2</sub>GaTaO<sub>6</sub> ( $\tau = 0.990$ ; Brandle & Fratello, 1990; Woodward *et al.*, 1994) and Sr<sub>2</sub>CrTaO<sub>6</sub> ( $\tau = 0.991$ ; Choy *et al.*, 1994; Woodward *et al.*, 1994) have both been reported as undistorted *Fm* $\bar{3}$ *m* cubic perovskites. Subsequently, Woodward (1997*c*) suggested that Sr<sub>2</sub>GaTaO<sub>6</sub> may not be cubic based on the observation that *R*-point reflections were present in a disordered sample. This suggests the presence of out-of-phase tilting. Subsequent Rietveld refinements carried out using XRPD data suggested an *a*<sup>0</sup>*a*<sup>0</sup>*c*<sup>-</sup> (*I4/m*) structure. However, the distinction between *a*<sup>0</sup>*a*<sup>0</sup>*a*<sup>0</sup> and *a*<sup>0</sup>*a*<sup>0</sup>*c*<sup>-</sup> can be very subtle in X-ray data and this assignment is difficult to confirm without neutron data.

The initial analysis of the XRPD and NPD diffraction data for Sr<sub>2</sub>GaTaO<sub>6</sub> and Sr<sub>2</sub>CrTaO<sub>6</sub> suggests that these compounds are cubic and isostructural with Ba<sub>2</sub>YNbO<sub>6</sub>. All of the superlattice reflections are of the *R*-type and there is negligible peak splitting, as shown in Fig. 3. Even though this suggests these two compounds have cubic structures, it does not exclude lower-symmetry structures that possess out-of-phase octahedral tilts. Rietveld refinements were carried out using *a*<sup>0</sup>*a*<sup>0</sup>*a*<sup>0</sup> (*Fm* $\bar{3}$ *m*), *a*<sup>0</sup>*a*<sup>0</sup>*c*<sup>-</sup> (*I4/m*) and *a*<sup>-</sup>*a*<sup>-</sup>*a*<sup>-</sup> (*R* $\bar{3}$ ) models. Unlike the Ba<sub>2</sub>YNbO<sub>6</sub> refinements, the intensities of the *R*-point reflections in the NPD patterns of Sr<sub>2</sub>GaTaO<sub>6</sub> and Sr<sub>2</sub>CrTaO<sub>6</sub> were poorly fit with the cubic model. The fit to these peaks was also unsatisfactory when using the rhombohedral *a*<sup>-</sup>*a*<sup>-</sup>*a*<sup>-</sup> (*R* $\bar{3}$ ) model. However, a good fit to the superlattice reflections could be obtained using the tetragonal *a*<sup>0</sup>*a*<sup>0</sup>*c*<sup>-</sup> (*I4/m*) model. The contrast between the cubic and tetragonal fits is shown in the inset to Fig. 4. A significant improvement can also be seen in the goodness-of-fit parameters for Sr<sub>2</sub>GaTaO<sub>6</sub>,  $\chi^2 = 5.11$  for the *Fm* $\bar{3}$ *m* model versus  $\chi^2 = 1.39$  for the *I4/m* model. For Sr<sub>2</sub>CrTaO<sub>6</sub> the goodness-of-fit parameters are  $\chi^2 = 4.03$  for the *Fm* $\bar{3}$ *m* model and  $\chi^2 = 2.56$  for the *I4/m* model. It should be pointed out that the inadequacy of the cubic model is difficult to see in the XRPD data, because the cation ordering contribution to the *R*-point reflections is much larger than the contribution from out-of-phase octahedral rotations. The apparent lack of reflection splitting can be appreciated from the values of the  $c/(2^{1/2}a)$  ratios: 0.9995 for Sr<sub>2</sub>CrTaO<sub>6</sub> and 0.9987 for Sr<sub>2</sub>GaTaO<sub>6</sub>. The small deviations from unity are not only because of the limited resolution of the neutron data. For example, the  $c/(2^{1/2}a)$  ratio for Sr<sub>2</sub>CrTaO<sub>6</sub> as determined from synchrotron X-ray powder diffraction data is 0.9996 (see details in §4). The refined crystal structures of Sr<sub>2</sub>GaTaO<sub>6</sub> and Sr<sub>2</sub>CrTaO<sub>6</sub> are given in Tables 2

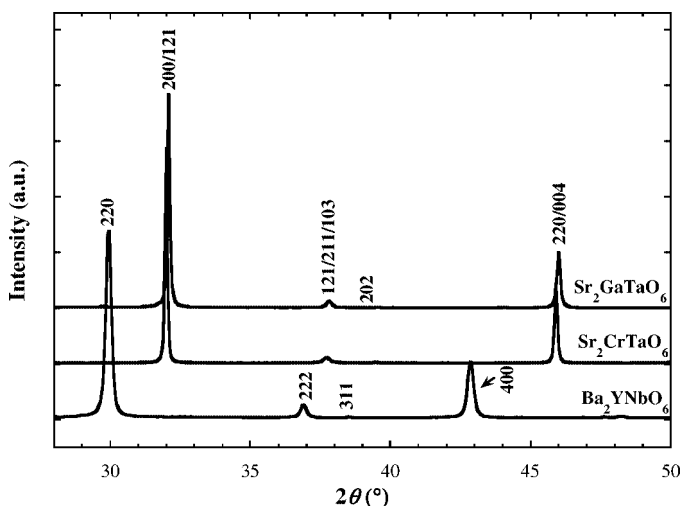


**Figure 3** Partial X-ray diffraction patterns for Ba<sub>2</sub>YNbO<sub>6</sub>, Sr<sub>2</sub>CrTaO<sub>6</sub> and Sr<sub>2</sub>GaTaO<sub>6</sub>. All superlattice reflections are of the *R*-type and no peak splitting is observed in any of the diffraction patterns over their entire 2θ range. Miller indices given above the diffraction data for Sr<sub>2</sub>GaTaO<sub>6</sub> are also applicable to Sr<sub>2</sub>CrTaO<sub>6</sub>.

and 3, and the  $I4/m$  structure is illustrated in Fig. 5. The Rietveld fit to the  $\text{Sr}_2\text{GaTaO}_6$  NPD data is shown in Fig. 4.

### 3.3. $\text{Sr}_2\text{ScNbO}_6$ , $\text{Ca}_2\text{AlTaO}_6$ and $\text{Ca}_2\text{CrTaO}_6$

The complete structure of  $\text{Sr}_2\text{ScNbO}_6$  ( $\tau = 0.963$ ) has not been reported previously, but monoclinic  $C2/c$  was suggested as a possible space group by Shan *et al.* (2001). This is a suspicious space-group assignment because the  $a^+b^+b^-$  ( $C2/c$ ) structure is one where there are multiple crystallographic sites

for the  $A$ -site cations (Howard *et al.*, 2003). As observed for the previous three compounds, both the XRPD and NPD patterns for  $\text{Sr}_2\text{ScNbO}_6$  appear cubic over the entire  $2\theta$  range (see Fig. 6). However, a significant number of superlattice reflections can be seen in both data sets. The inset to Fig. 7 focuses on the superlattice reflections in the neutron pattern at  $35.2$ ,  $37.0$ ,  $40.4$ ,  $42.0$ ,  $46.3$ ,  $49.3$  and  $59.7^\circ 2\theta$ . The reflections that fall at  $37.0$ ,  $49.3$  and  $59.7^\circ$  can be indexed as the 311, 331 and 511/333 reflections on the double-edge cubic cell, respectively. These  $R$ -point reflections are the strongest set of superlattice peaks. In a manner analogous to that used in the analysis of the previous three compounds, the reflections signify out-of-phase tilting, rock-salt cation ordering or both. The reflections that fall at  $35.2$  and  $42.0^\circ 2\theta$  can be indexed with the cubic cell as the 310 and 321 reflections. These belong to the somewhat weaker set of  $M$ -point reflections which unambiguously indicate in-phase octahedral tilting. Finally, the weakest set of superlattice peaks falls at  $40.4$  and  $46.3^\circ$ , which correspond to the 320 and 410/322 double-edge cubic cell reflections. These are  $X$ -point reflections that generally are indicative of  $A$ -site cation displacements that arise from the coupling of in-phase and out-of-phase tilts. Therefore, these peaks serve as an indirect indicator of out-of-phase tilts. In the XRPD data the  $X$ -point reflections are more intense than the  $M$ -point peaks due to the enhanced scattering power of strontium and the diminished scattering power of oxygen. Of the three possible tilt systems that combine in-phase and out-of-phase tilts the  $a^-a^-c^+$  ( $P2_1/n$ ) structure is the most common. Furthermore, the tolerance factor (Goldschmidt, 1926),  $\tau = 0.963$ , is in the range where the  $a^-a^-c^+$  ( $P2_1/n$ ) structure is expected. Rietveld refinements confirm this assignment. The refined crystal structure of  $\text{Sr}_2\text{ScNbO}_6$  is given in Table 4, while the Rietveld fit of the NPD data set is shown in Fig. 7.

The earliest reports of  $\text{Ca}_2\text{AlNbO}_6$  ( $\tau = 0.963$ ) and  $\text{Ca}_2\text{CrTaO}_6$  ( $\tau = 0.937$ ) are by

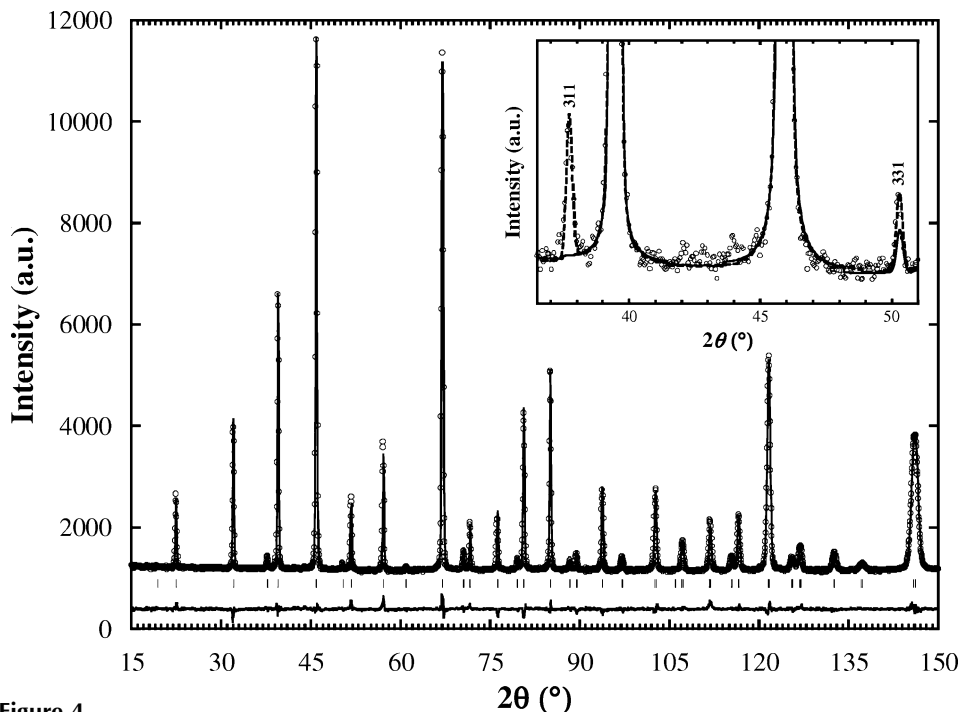


**Figure 4**  
Observed neutron diffraction pattern along with calculated and difference patterns from the Rietveld refinement of  $\text{Sr}_2\text{GaTaO}_6$ . The vertical tick marks indicate the expected  $2\theta$  position of the reflections. Inset: Comparison of the calculated patterns for an  $Fm\bar{3}m$  model (solid line;  $\chi^2 = 5.11$ ) and the  $I4/m$  model (dashed line;  $\chi^2 = 1.39$ ). The Miller indices included in the inset are those for the double-edge cubic cell.

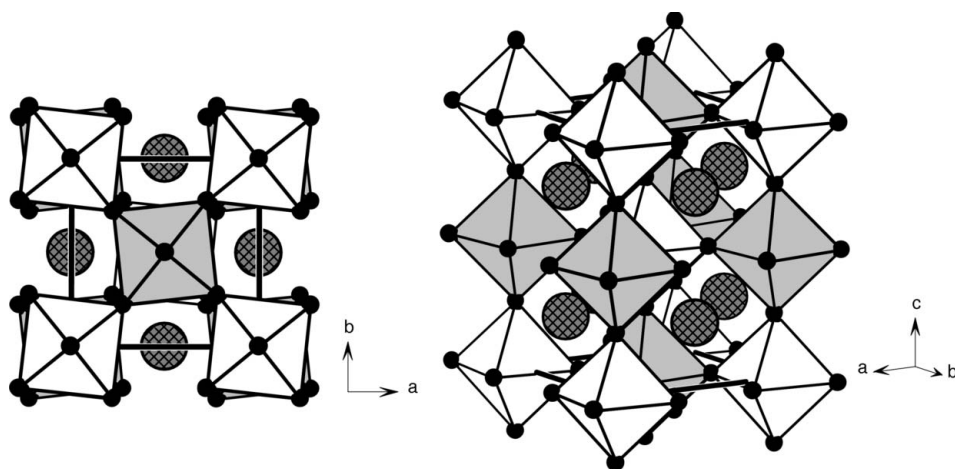


**Figure 5**  
The structure of  $\text{Sr}_2\text{GaTaO}_6$  (space group  $I4/m$ ; tilt system:  $a^0a^0c^-$ ). Octahedral tilting occurs along the  $z$  axis, as shown in Fig. 4. Legend:  $[\text{CrO}_6]$ : white octahedra;  $[\text{TaO}_6]$ : grey octahedra; Sr: cross-hatched spheres; O – filled spheres.

**Table 2**

The crystal structure of  $\text{Sr}_2\text{GaTaO}_6$  as determined from neutron powder diffraction data.

The space-group symmetry is  $I4/m$ . The unit-cell dimensions are  $a = 5.5754$  (1) and  $c = 7.8949$  (2) Å. The goodness-of-fit parameters are  $R_p = 0.0374$ ,  $R_{wp} = 0.0482$  and  $\chi^2 = 1.39$ .

	Site	$x$	$y$	$z$	$U_{\text{iso}}$ (Å <sup>2</sup> )
Sr	4( <i>d</i> )	0	1/2	1/4	0.0112 (2)
Ga	2( <i>a</i> )	0	0	0	0.0064 (2)
Ta	2( <i>b</i> )	1/2	1/2	0	0.0034 (2)
O1	4( <i>e</i> )	0	0	0.2499 (7)	0.0097 (7)
O2	8( <i>h</i> )	0.2671 (5)	0.2327 (5)	0	0.0116 (3)

**Table 3**

Crystal structure of  $\text{Sr}_2\text{CrTaO}_6$  as determined from neutron powder diffraction data.

The space-group symmetry is  $I4/m$ . The unit-cell dimensions are  $a = 5.5752$  (2) and  $c = 7.8808$  (5) Å. The goodness-of-fit parameters are  $R_p = 0.0706$ ,  $R_{wp} = 0.0924$  and  $\chi^2 = 2.56$ .

	Site	$x$	$y$	$z$	Occupancy	$U_{\text{iso}}$ (Å <sup>2</sup> )
Sr	4( <i>d</i> )	0	1/2	1/4	1	0.0143 (5)
Cr	2( <i>a</i> )	0	0	0	0.80 (2)	0.0076 (6)†
Ta	2( <i>a</i> )	0	0	0	0.20	0.0076†
Ta	2( <i>b</i> )	1/2	1/2	0	0.80	0.0076†
Cr	2( <i>b</i> )	1/2	1/2	0	0.20	0.0076†
O1	4( <i>e</i> )	0	0	0.2501 (9)	1	0.010 (3)
O2	8( <i>h</i> )	0.2655 (6)	0.2342 (8)	0	1	0.011 (2)

† In order to avoid unwanted correlations with the order parameter the  $U_{\text{iso}}$  values for octahedral site cations were constrained to be equal.

Filip'ev & Fesenko (1966), who described both compounds as orthorhombic. More recently the structures of  $\text{Ca}_2\text{CrTaO}_6$  (Choy *et al.*, 1994) and  $\text{Ca}_2\text{AlNbO}_6$  (Vanderah *et al.*, 2000; Levin, Chan, Maslar, Vanderah & Bell, 2001) have been reported with the  $a^-a^-c^+$  ( $P2_1/n$ ) structure. Our analysis agrees with these later reports. We report our results in order to contrast the analysis with the more highly pseudo-cubic  $\text{Sr}_2\text{ScNbO}_6$ .

The fundamental reflection splitting in  $\text{Sr}_2\text{ScNbO}_6$ ,  $\text{Ca}_2\text{AlNbO}_6$  and  $\text{Ca}_2\text{CrTaO}_6$  X-ray diffraction data is shown in Fig. 6. The reflection splitting observed in the latter two compounds can be easily seen and matches the pattern expected for a perovskite with a pseudo-orthorhombic  $2^{1/2}a_p \times 2^{1/2}a_p \times 2a_p$  unit cell ( $a_p$  is the simple cubic  $AMX_3$  cell edge). The observation of a unit cell with an orthorhombic metric can lead to errors in the space-group assignment, particularly in the older literature. However, the group-theoretical treatment (Howard *et al.*, 2003) shows that no structures with  $2^{1/2}a_p \times 2^{1/2}a_p \times 2a_p$  unit-cell and orthorhombic symmetry result from the combination of octahedral tilting and rock-salt ordering. The reflection splitting seen in Fig. 6 matches the splitting pattern for two different tilt systems:  $a^-a^-c^+$  ( $P2_1/n$ ) and  $a^0b^-b^-$  ( $I2/m$ ). These two structures can be differentiated by analysis of the superlattice reflections. The NPD patterns of both  $\text{Ca}_2\text{AlNbO}_6$  (Fig. 8) and  $\text{Ca}_2\text{CrTaO}_6$  (Fig. 9) show all three types of superlattice reflections, consistent with the  $a^-a^-c^+$  ( $P2_1/n$ ) structure

**Table 4**

The crystal structure of  $\text{Sr}_2\text{ScNbO}_6$  as determined from neutron powder diffraction data.

The space-group symmetry is  $P2_1/n$ . The unit-cell dimensions are  $a = 5.7045$  (2),  $b = 5.6973$  (2),  $c = 8.0505$  (2) Å and  $\beta = 90.021$  (8)°. The goodness-of-fit parameters are  $R_p = 0.0433$ ,  $R_{wp} = 0.0546$  and  $\chi^2 = 1.68$ .

	Site	$x$	$y$	$z$	Occupancy	$U_{\text{iso}}$ (Å <sup>2</sup> )
Sr	4( <i>e</i> )	0.5026 (8)	0.5118 (5)	0.247 (2)	1	0.0117 (3)
Sc	2( <i>c</i> )	0	1/2	0	0.78 (1)	0.0078 (1)†
Nb	2( <i>c</i> )	0	1/2	0	0.22	0.0078†
Nb	2( <i>d</i> )	1/2	0	0	0.78	0.0078†
Sc	2( <i>d</i> )	1/2	0	0	0.22	0.0078†
O1	4( <i>e</i> )	0.2356 (9)	0.225 (1)	-0.0237 (7)	1	0.008 (1)
O2	4( <i>e</i> )	0.279 (1)	0.726 (1)	-0.0313 (7)	1	0.0127 (2)
O3	4( <i>e</i> )	0.4441 (6)	-0.0057 (7)	0.2458 (7)	1	0.0114 (6)

† In order to avoid unwanted correlations with the order parameter the  $U_{\text{iso}}$  values for the octahedral site cations were constrained to be equal.

(shown in Fig. 10). The refined structures of these two compounds are given in Tables 5 and 6. Even when the symmetry is lowered to monoclinic the deviation of the  $\beta$  angles from 90° is negligible, 89.970 (4)° for  $\text{Ca}_2\text{AlNbO}_6$  and 90.014 (5)° for  $\text{Ca}_2\text{CrTaO}_6$ .

### 3.4. XRPD analysis of additional $A_2MTaO_6$ and $A_2MNbO_6$ compounds

The preceding sections show how neutron powder diffraction data can be of great help when identifying the presence and type of octahedral tilting. Nonetheless, NPD data is not always available or suitable for certain elements. When NPD is not available, careful analysis of the superlattice reflections and fundamental reflection splitting in high-quality XRPD data can be used to correctly identify the tilt system and space group in all but the most pathological cases. Of the six compounds whose structures are discussed above, only the  $I4/m$  compounds with pseudo-cubic cells,  $\text{Sr}_2\text{GaTaO}_6$  and  $\text{Sr}_2\text{CrTaO}_6$ , have structures that cannot be identified in a

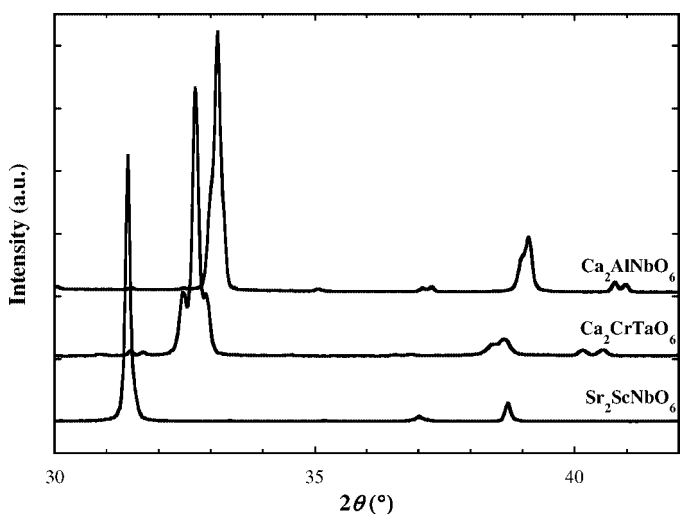


**Figure 6**  
Partial X-ray diffraction patterns for  $\text{Sr}_2\text{ScNbO}_6$ ,  $\text{Ca}_2\text{CrTaO}_6$  and  $\text{Ca}_2\text{AlNbO}_6$ .

**Table 5**

The crystal structure of  $\text{Ca}_2\text{CrTaO}_6$  as determined from neutron powder diffraction data.

The space-group symmetry is  $P2_1/n$ . The unit-cell dimensions are  $a = 5.42456$  (7),  $b = 5.49772$  (6),  $c = 7.7166$  (1) Å and  $\beta = 90.014$  (5)°. The goodness-of-fit parameters are  $R_p = 0.0424$ ,  $R_{\text{wp}} = 0.0544$  and  $\chi^2 = 1.40$ . The refinements showed 3 (1)%  $\text{Ca}_3(\text{CaTa}_2)\text{O}_9$  was present.

Site	<i>x</i>	<i>y</i>	<i>z</i>	Occupancy	$U_{\text{iso}}$ (Å <sup>2</sup> )	
Ca	4( <i>e</i> )	0.5055 (3)	0.5382 (2)	0.249 (1)	1	0.0124 (3)
Cr	2( <i>c</i> )	0	1/2	0	0.80 (1)	0.0043 (3)†
Ta	2( <i>c</i> )	0	1/2	0	0.20	0.0043†
Ta	2( <i>d</i> )	1/2	0	0	0.80	0.0043†
Cr	2( <i>d</i> )	1/2	0	0	0.20	0.0043†
O1	4( <i>e</i> )	0.2079 (8)	0.2089 (7)	−0.0370 (5)	1	0.015 (1)
O2	4( <i>e</i> )	0.2931 (7)	0.7077 (6)	−0.0435 (5)	1	0.0002 (8)
O3	4( <i>e</i> )	0.4224 (2)	−0.0194 (2)	0.2518 (8)	1	0.0059 (3)

† In order to avoid unwanted correlations with the order parameter the  $U_{\text{iso}}$  values for the octahedral site cations were constrained to be equal.

straightforward manner through a careful analysis of XRPD data. In the course of this work, high-resolution laboratory or synchrotron X-ray powder diffraction data (as described in §2) were collected on a number of additional  $A_2MTaO_6$  and  $A_2MNbO_6$  compounds. These data sets were analyzed using the Rietveld method. The space group, unit-cell dimensions and cation ordering characteristics are reported in Table 7. The synthetic conditions used to prepare these compounds are reported elsewhere (Woodward, 1997c; Barnes, 2003). The atomic coordinates are not reported because the pseudosym-

**Table 6**

The crystal structure of  $\text{Ca}_2\text{AlNbO}_6$  as determined from neutron powder diffraction data.

The space-group symmetry is  $P2_1/n$ . The unit-cell dimensions are  $a = 5.37706$  (9),  $b = 5.41557$  (9),  $c = 7.6255$  (1) Å and  $\beta = 89.970$  (4)°. The goodness-of-fit parameters are  $R_p = 0.0402$ ,  $R_{\text{wp}} = 0.0522$  and  $\chi^2 = 1.49$ .

Site	<i>x</i>	<i>y</i>	<i>z</i>	Occupancy	$U_{\text{iso}}$ (Å <sup>2</sup> )	
Ca	4( <i>e</i> )	0.5059 (4)	0.5309 (2)	0.2484 (8)	1	0.0116 (3)
Al	2( <i>c</i> )	0	1/2	0	0.941 (8)	0.0037 (2)†
Nb	2( <i>c</i> )	0	1/2	0	0.059	0.0037†
Nb	2( <i>d</i> )	1/2	0	0	0.941	0.0037†
Al	2( <i>d</i> )	1/2	0	0	0.059	0.0037†
O1	4( <i>e</i> )	0.2092 (6)	0.2158 (7)	−0.0340 (5)	1	0.0063 (8)
O2	4( <i>e</i> )	0.2824 (6)	0.7130 (8)	−0.0338 (5)	1	0.0091 (8)
O3	4( <i>e</i> )	0.4333 (2)	−0.0131 (2)	0.2529 (6)	1	0.0085 (3)

† In order to avoid unwanted correlations with the order parameter, the  $U_{\text{iso}}$  values for the octahedral site cations were constrained to be equal.

metry makes it difficult to obtain highly accurate values for the oxygen coordinates from analysis of the X-ray data.

Most of the  $A_2MTaO_6$  and  $A_2MNbO_6$  compounds investigated exhibited partial ordering of the *M* and *M'* cations. Partial ordering was accounted for in the Rietveld refinements using the constraints described in §2.3. The degree of cation ordering is quantified with the long-range order parameter, LRO

$$\text{LRO} = [2 \times (\text{occ.})_M - 1] \times 100$$

where  $(\text{occ.})_M$  is the fractional occupancy of the Ta or Nb cation on the octahedral site that is predominantly occupied

by that cation (Sleight, 1963; Woodward *et al.*, 1994). For example, in  $\text{Sr}_2\text{CrTaO}_6$  the site preferentially occupied by tantalum contains 80%  $\text{Ta}^{5+}$  and 20%  $\text{Cr}^{3+}$ . Therefore, the LRO parameter is  $[2 \times 0.80 - 1] \times 100 = 60\%$ . Table 7 contains long-range order parameters for several  $A_2MTaO_6$  and  $A_2MNbO_6$  compounds, as determined from the X-ray data. Note that the six compounds whose structures are reported in §§3.1–3.3 are also included, but the results reported in Table 7 are obtained from the analysis of XRPD data rather than NPD data. Discrepancies between the order parameters reported in Table 7 and those reported in Tables 2–6 can be attributed to differences in the neutron and X-ray scattering powers of the elements. For the compounds studied in this work the *M/M'* scattering contrast is generally larger for X-rays. Consequently, the values

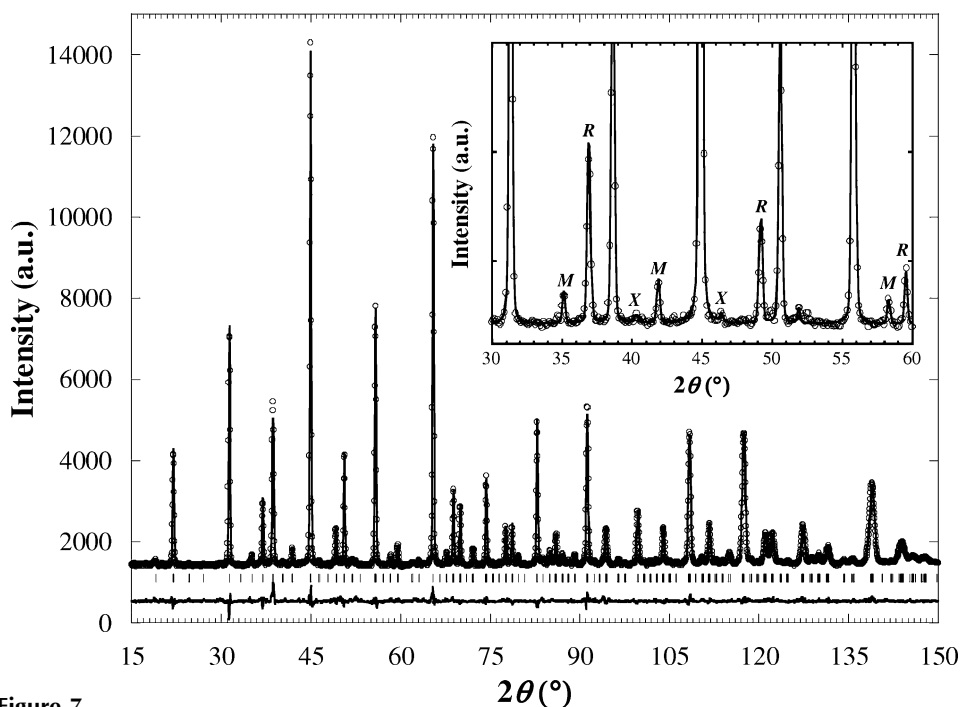


**Figure 7**

Observed neutron diffraction pattern along with calculated and difference patterns from the Rietveld refinement of  $\text{Sr}_2\text{ScNbO}_6$ . Vertical bars shown between the fit data and difference patterns indicate the  $2\theta$  position of the observed reflections. The inset emphasizes key superstructure reflections due to in-phase octahedral tilting (marked *M*), out-of-phase tilting (*R*) and coupled in-phase and out-of-phase tilting (*X*).

**Table 7**

Space groups, unit-cell parameters, and cation ordering characteristics for perovskite compositions containing either Nb<sup>5+</sup> or Ta<sup>5+</sup>, as obtained from analysis of either synchrotron or monochromatic laboratory X-ray powder diffraction data.

Compound	$\tau^\dagger$	$\Delta r$ (Å) <sup>‡</sup>	Space group	$a$ (Å)	$b$ (Å)	$c$ (Å)	$\beta$ (°)	$D$ <sup>§</sup> (%)	LRO (%)
Ba <sub>2</sub> ScNbO <sub>6</sub>	1.021	+0.105	<i>Fm</i> $\bar{3}$ <i>m</i>	8.23402 (7)	–	–	–	0	53 (2)
Ba <sub>2</sub> ScTaO <sub>6</sub>	1.020	+0.105	<i>Fm</i> $\bar{3}$ <i>m</i>	8.23147 (5)	–	–	–	0	51 (1)
Sr <sub>2</sub> GaNbO <sub>6</sub>	0.992	–0.020	<i>I4</i> / <i>m</i>	5.57454 (2)	–	7.89566 (6)	–	0.07	57 (3)
Sr <sub>2</sub> CrTaO <sub>6</sub> <sup>¶</sup>	0.991	–0.025	<i>I4</i> / <i>m</i>	5.58318 (7)	–	7.8927 (2)	–	0.05	62 (1)
Sr <sub>2</sub> GaTaO <sub>6</sub>	0.990	–0.020	<i>I4</i> / <i>m</i>	5.57686 (3)	–	7.89684 (7)	–	0.17	77 (1)
Sr <sub>2</sub> VTaO <sub>6</sub> <sup>¶</sup>	0.986	0.000	<i>I4</i> / <i>m</i>	5.60363 (4)	–	7.94513 (8)	–	0.11	50 (1)
Ba <sub>2</sub> YNbO <sub>6</sub>	0.980	+0.260	<i>Fm</i> $\bar{3}$ <i>m</i>	8.44073 (6)	–	–	–	0	100
Sr <sub>2</sub> RhTaO <sub>6</sub> <sup>¶</sup>	0.974	+0.025	<i>I4</i> / <i>m</i>	5.61424 (3)	–	7.91732 (9)	–	0.13	70 (1)
Ca <sub>2</sub> AlNbO <sub>6</sub>	0.963	–0.105	<i>P2</i> <sub>1</sub> / <i>n</i>	5.37443 (6)	5.41386 (6)	7.62197 (9)	89.955 (1)	0.26	87 (1)
Sr <sub>2</sub> ScNbO <sub>6</sub>	0.963	+0.105	<i>P2</i> <sub>1</sub> / <i>n</i>	5.6967 (2)	5.6959 (2)	8.0451 (2)	90.059 (8)	0.18	69 (1)
Sr <sub>2</sub> ScTaO <sub>6</sub>	0.961	+0.105	<i>P2</i> <sub>1</sub> / <i>n</i>	5.6955 (3)	5.6982 (2)	8.0625 (5)	90.00††	0.10	71 (1)
Sr <sub>2</sub> InNbO <sub>6</sub>	0.951	+0.160	<i>P2</i> <sub>1</sub> / <i>n</i>	5.73273 (4)	5.74838 (4)	8.10700 (8)	90.043 (1)	0.12	80 (3)
Sr <sub>2</sub> InTaO <sub>6</sub>	0.949	+0.160	<i>P2</i> <sub>1</sub> / <i>n</i>	5.73307 (3)	5.74041 (3)	8.10826 (5)	90.011 (2)	0.06	86 (1)
Ca <sub>2</sub> CrTaO <sub>6</sub> <sup>¶</sup>	0.937	–0.025	<i>P2</i> <sub>1</sub> / <i>n</i>	5.42870 (5)	5.50201 (5)	7.72254 (7)	90.031 (5)	1.40	56 (1)
Ca <sub>2</sub> GaTaO <sub>6</sub>	0.936	–0.020	<i>P2</i> <sub>1</sub> / <i>n</i>	5.43228 (4)	5.51024 (4)	7.72365 (6)	89.990 (6)	0.51	48 (1)
Ca <sub>2</sub> ScNbO <sub>6</sub>	0.911	+0.105	<i>P2</i> <sub>1</sub> / <i>n</i>	5.51222 (9)	5.63333 (4)	7.8688 (1)	89.995 (6)	0.76	96 (1)
Ca <sub>2</sub> ScTaO <sub>6</sub>	0.909	+0.105	<i>P2</i> <sub>1</sub> / <i>n</i>	5.51119 (4)	5.64070 (4)	7.87187 (6)	89.989 (3)	0.81	90 (1)
Ca <sub>2</sub> InTaO <sub>6</sub>	0.897	+0.160	<i>P2</i> <sub>1</sub> / <i>n</i>	5.52884 (3)	5.70805 (3)	7.92248 (5)	90.097 (1)	1.13	100
Ca <sub>2</sub> YNbO <sub>6</sub>	0.878	+0.260	<i>P2</i> <sub>1</sub> / <i>n</i>	5.58148 (2)	5.80933 (2)	8.05178 (4)	90.040 (1)	1.34	100‡‡

† Bond-valence parameter tolerance factors were calculated using *SPuDS*. ‡  $\Delta r = r(M^{3+}) - r(M^{5+})$ . §  $D$  is a measure of the distortion of the unit cell.  $D = \Sigma[|a_{pc}(i) - a_{pc}(avg)|] / \Sigma\{a_{pc}(i)\}$ , where  $a_{pc}(i)$  are the pseudo-cubic values of the cell edges ( $\sim 8$  Å) and  $a_{pc}(avg)$  is the volume average pseudo-cubic cell edge. ¶ Diffraction data collected at the National Synchrotron Light Source, Brookhaven National Laboratory, beamline X7A. If not marked, XRPD was collected on a Bruker Advance D8 X-ray diffractometer as described in §2. ††  $\beta$  could not be refined for Sr<sub>2</sub>ScTaO<sub>6</sub>, so its value was fixed at 90°. ‡‡ In Ca<sub>2</sub>YNbO<sub>6</sub> there is mixing of Ca<sup>2+</sup> and Y<sup>3+</sup>, but the Nb<sup>5+</sup> site is fully occupied by Nb<sup>5+</sup>.

reported in Table 7 are thought to be a more accurate assessment of cation ordering in these compounds.

Broadening of the superlattice reflections indicate the presence of anti-phase boundaries in the  $M/M'$  cation distribution (Woodward *et al.*, 1994). APBs are extended defects

that occur when out-of-phase ordered domains that have nucleated independently grow together. APBs can be detected in the powder diffraction data when the ordered domain size becomes small enough to cause extra size broadening of the cation ordering contribution to the  $R$ -point reflections. Among

the compounds examined in this study, some degree of broadening of the  $R$ -point superlattice reflections was observed for all  $A_2MM'O_6$  perovskites that exhibit partial cation order.

#### 4. Discussion

Selected bond distances and angles, along with bond-valence sums (Brown & Altermatt, 1985), octahedron distortion indices and polyhedral volumes ( $V_A$ ,  $V_M$  and  $V_A/V_M$ ) are reported in Table 8. The bond-valence sums for the constituent ions are very close to their ideal values. For the purposes of these calculations the presence of disorder has been neglected, although it is acknowledged that when present it may cause some deviation from ideal values. The overall agreement with expected values is a good indication that the octahedral tilting distortions in these compounds have been modeled appropriately and that the

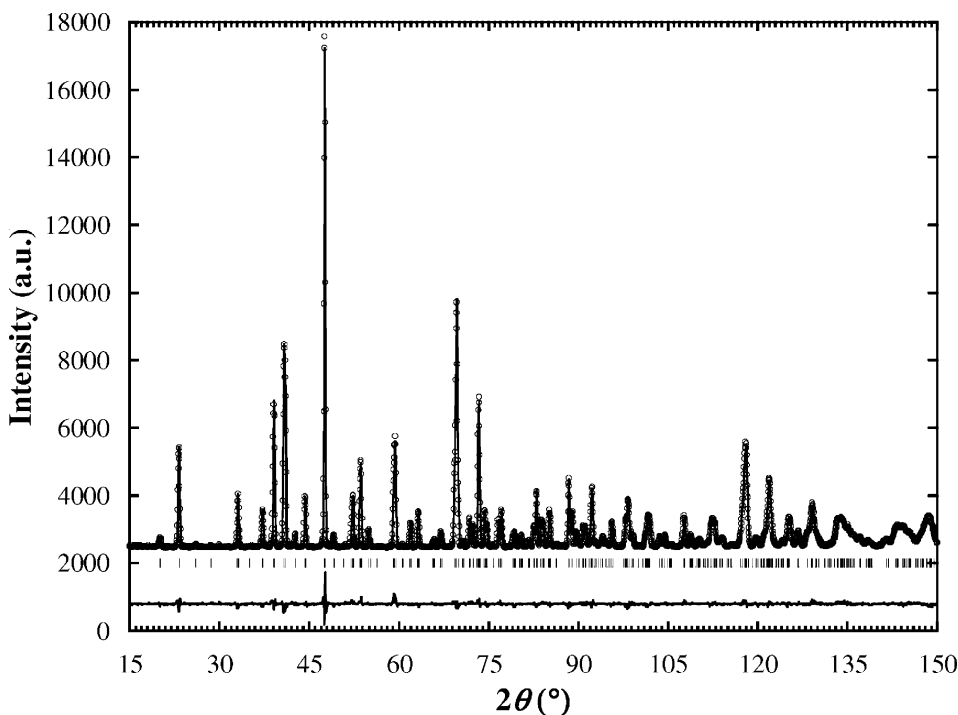


**Figure 8** Observed neutron diffraction pattern along with calculated and difference patterns from the Rietveld refinement of Ca<sub>2</sub>AlNbO<sub>6</sub>. Vertical bars shown between the fit data and difference patterns indicate the  $2\theta$  position of the observed reflections.

**Table 8**

Selected bond distances and angles, bond-valence sums, octahedron distortion indices and polyhedral volumes, as determined from the crystallographic data reported in Tables 2–7.

	Sr <sub>2</sub> CrTaO <sub>6</sub>	Sr <sub>2</sub> GaTaO <sub>6</sub>	Ba <sub>2</sub> YNbO <sub>6</sub>	Sr <sub>2</sub> ScNbO <sub>6</sub>	Ca <sub>2</sub> AlNbO <sub>6</sub>	Ca <sub>2</sub> CrTaO <sub>6</sub>
Bond distances (Å) and angles (°)						
A–O1	4 × 2.7876 (1)	4 × 2.7877 (5) 1	2 × 2.98636 (5)	2.64 (1) 2.78 (1) 2.88 (1)	2.395 (6) 2.627 (6) 2.660 (7)	2.405 (6) 2.651 (6) 2.678 (8)
A–O2	4 × 2.7008 (2) 4 × 2.8758 (2)	4 × 2.6952 (8) 4 × 2.8871 (9)	–	2.53 (1) 2.81 (1) 2.85 (1)	2.391 (6) 2.626 (6) 2.655 (7)	2.353 (6) 2.638 (6) 2.699 (7)
A–O3	–	–	–	2.55 (6) 2.76 (5) 2.96 (5)	2.373 (2) 2.501 (2) 2.972 (2)	2.343 (2) 2.475 (2) 3.120 (2)
M <sup>3+</sup> –O1	2 × 1.970 (5)	2 × 1.973 (6)	6 × 2.2188 (7)	2 × 2.073 (4)	2 × 1.924 (3)	2 × 1.979 (4)
M <sup>3+</sup> –O2	4 × 1.976 (3)	4 × 1.975 (4)	–	2 × 2.063 (4)	2 × 1.924 (3)	2 × 1.987 (4)
M <sup>3+</sup> –O3	–	–	–	2 × 2.072 (4)	2 × 1.919 (5)	2 × 1.964 (6)
M <sup>5+</sup> –O1	2 × 1.971 (7)	2 × 1.974 (7)	6 × 2.0018 (7)	2 × 1.989 (4)	2 × 1.969 (3)	2 × 1.978 (4)
M <sup>5+</sup> –O2	4 × 1.974 (5)	4 × 1.976 (5)	–	2 × 2.022 (4)	2 × 1.963 (3)	2 × 1.989 (4)
M <sup>5+</sup> –O3	–	–	–	2 × 2.004 (5)	2 × 1.963 (5)	2 × 1.992 (6)
M <sup>3+</sup> –O1–M <sup>5+</sup>	180	180	180	166.0 (3)	157.1 (2)	154.9 (2)
M <sup>3+</sup> –O2–M <sup>5+</sup>	172.8 (2)	172.11 (7)	–	161.3 (3)	158.1 (3)	152.6 (2)
M <sup>3+</sup> –O3–M <sup>5+</sup>	–	–	–	161.9 (2)	158.3 (1)	154.6 (6)
Bond-valence sums						
A	2.00	2.00	1.80	2.00	2.05	1.97
M <sup>3+</sup>	3.05	3.10	3.50	3.17	2.65	3.03
M <sup>5+</sup>	5.20	5.17	4.70	4.87	5.19	5.02
O1	2.04	2.04	1.96	1.97	1.97	1.97
O2	2.04	2.05	–	2.08	1.99	1.98
O3	–	–	–	1.98	2.01	2.05
Distortion indices, Δ <sub>d</sub> (× 10 <sup>−5</sup> )†						
M <sup>3+</sup>	0.21	0.02	–	1.88	0.15	2.33
M <sup>5+</sup>	0.05	0.02	–	5.33	0.21	0.92
Polyhedral volumes						
V <sub>A</sub>	51.0 (1)	51.1 (1)	62.6 (1)	55.1 (3)	47.1 (1)	48.8 (1)
V <sub>M<sup>3+</sup></sub>	10.24 (3)	10.27 (2)	14.57 (2)	11.80 (6)	9.48 (3)	10.28 (4)
V <sub>M<sup>5+</sup></sub>	10.26 (3)	10.28 (2)	10.69 (2)	10.75 (5)	10.11 (4)	10.45 (4)
V <sub>A</sub> /V <sub>M</sub> (AVG)	4.98	4.97	4.96	4.89	4.81	4.71

† Δ<sub>d</sub> is the octahedral distortion index, Δ<sub>d</sub> = 1/6 ∑<sub>n=1,6</sub> [d<sub>n</sub> − ⟨d⟩/⟨d⟩]<sup>2</sup>, where the individual M–O bond distances are given by d<sub>n</sub> and ⟨d⟩ is the average M–O bond length.

proposed crystal structures are indeed correct.

Regularity of the octahedra can be quantified using the distortion index, Δ<sub>d</sub> (Alonso *et al.*, 2000). Octahedra with significant distortions, such as those observed around Mn<sup>3+</sup> in the rare-earth manganate perovskites, have values of Δ<sub>d</sub> that range from 3.3 × 10<sup>−3</sup> to 5.0 × 10<sup>−3</sup> (Alonso *et al.*, 2000). In the compounds studied here there are no strong electronic factors favoring distortions of the octahedra and small Δ<sub>d</sub> values are expected. Octahedral tilting distortions are typically assumed to occur between ideal, rigid octahedra. If this assumption were rigorously true, the distortion indexes would all be zero, but considering the relatively low space-group symmetry non-zero values are expected. As shown in Table 8, the octahedral distortion indices for the compounds examined in this study are comparatively small. This result, coupled with the small deviations of the O–M–O bond angles from 90°, validates the basic assumption that these distortions can be described as tilting of regular octahedra.

Polyhedral volumes (V<sub>A</sub>, V<sub>M</sub> and V<sub>A</sub>/V<sub>M</sub>) were calculated for all compositions using the *IVTON* software (Balić Žunić & Makovicky, 1996). In ternary AMX<sub>3</sub> perovskites, Thomas (1989) has shown that the ratio V<sub>A</sub>/V<sub>M</sub> is strictly equal to 5 in

the cubic aristotype structure. This ratio is generally less than 5 in distorted perovskites and it decreases as the magnitude of the octahedral tilting distortion increases (Thomas, 1996*a,b*). Among the compounds analyzed by Thomas, a<sup>−</sup>a<sup>−</sup>c<sup>+</sup> tilting is observed for 4.9 > V<sub>A</sub>/V<sub>M</sub> > 4.1, and is strongly favored when V<sub>A</sub>/V<sub>M</sub> < 4.7. The V<sub>A</sub>/V<sub>M</sub> ratio of 4.89 observed for Sr<sub>2</sub>ScNbO<sub>6</sub> suggests that a transition to a higher-symmetry tilt system is likely to occur upon heating. It would be interesting to collect structural data as a function of temperature for this compound to see how the pseudosymmetry evolves over a wide temperature range.

A list of the structures of 32 perovskites containing Nb<sup>5+</sup> or Ta<sup>5+</sup> is given in Table 9. Examination of this table allows several empirical generalizations to be made about octahedral tilting distortions in double perovskites containing Nb<sup>5+</sup> or Ta<sup>5+</sup>. When the tolerance factor, τ, is greater than unity the cubic structure is strongly favored. When the tolerance factor is between 0.98 and 1, octahedral tilting distortions tend to occur. In this narrow range, a variety of tilt systems are observed, including a<sup>0</sup>a<sup>0</sup>a<sup>0</sup>, a<sup>0</sup>a<sup>0</sup>c<sup>−</sup> and a<sup>−</sup>a<sup>−</sup>c<sup>+</sup>. When the tolerance factor falls below 0.98 the a<sup>−</sup>a<sup>−</sup>c<sup>+</sup> tilt system is seen almost exclusively. These trends are in line with the findings of

**Table 9**

A comparison of space group *versus* tolerance factor for 32 different compounds containing Nb<sup>5+</sup> or Ta<sup>5+</sup>.

Compound	$\tau$	Space group	Tilt system†	Cation ordering	Diffraction type	Reference
Ba <sub>2</sub> FeNbO <sub>6</sub>	1.044	<i>Fm</i> $\bar{3}$ <i>m</i>	<i>a</i> <sup>0</sup> <i>a</i> <sup>0</sup> <i>a</i> <sup>0</sup>	Yes	XRPD	(a)
Ba <sub>2</sub> FeTaO <sub>6</sub>	1.042	<i>Pm</i> $\bar{3}$ <i>m</i>	<i>a</i> <sup>0</sup> <i>a</i> <sup>0</sup> <i>a</i> <sup>0</sup>	No	XRPD	(b)
Ba <sub>2</sub> ScNbO <sub>6</sub>	1.021	<i>Fm</i> $\bar{3}$ <i>m</i>	<i>a</i> <sup>0</sup> <i>a</i> <sup>0</sup> <i>a</i> <sup>0</sup>	Yes	XRPD	(c)
Sr <sub>2</sub> AlNbO <sub>6</sub>	1.020	<i>Fm</i> $\bar{3}$ <i>m</i>	<i>a</i> <sup>0</sup> <i>a</i> <sup>0</sup> <i>a</i> <sup>0</sup>	Yes	XRPD	(d)
Ba <sub>2</sub> ScTaO <sub>6</sub>	1.019	<i>Fm</i> $\bar{3}$ <i>m</i>	<i>a</i> <sup>0</sup> <i>a</i> <sup>0</sup> <i>a</i> <sup>0</sup>	Yes	XRPD	(b)
Sr <sub>2</sub> CoNbO <sub>6</sub>	1.016	<i>Pm</i> $\bar{3}$ <i>m</i>	<i>a</i> <sup>0</sup> <i>a</i> <sup>0</sup> <i>a</i> <sup>0</sup>	No	XRPD	(e)
Sr <sub>2</sub> AlTaO <sub>6</sub>	1.018	<i>Fm</i> $\bar{3}$ <i>m</i>	<i>a</i> <sup>0</sup> <i>a</i> <sup>0</sup> <i>a</i> <sup>0</sup>	Yes	NPD	(d)
Sr <sub>2</sub> CoTaO <sub>6</sub>	1.013	<i>I4/mcm</i>	<i>a</i> <sup>0</sup> <i>a</i> <sup>0</sup> <i>c</i> <sup>-</sup>	No	XRPD	(b)
Ba <sub>2</sub> InTaO <sub>6</sub>	1.006	<i>Fm</i> $\bar{3}$ <i>m</i>	<i>a</i> <sup>0</sup> <i>a</i> <sup>0</sup> <i>a</i> <sup>0</sup>	Yes	XRPD	(b)
Sr <sub>2</sub> CrTaO <sub>6</sub>	0.991	<i>I4/m</i>	<i>a</i> <sup>0</sup> <i>a</i> <sup>0</sup> <i>c</i> <sup>-</sup>	Yes	NPD	(b), (f)
Sr <sub>2</sub> GaTaO <sub>6</sub>	0.990	<i>I4/m</i>	<i>a</i> <sup>0</sup> <i>a</i> <sup>0</sup> <i>c</i> <sup>-</sup>	Yes	NPD	(f)
Sr <sub>2</sub> MnNbO <sub>6</sub>	0.985	<i>I4/mcm</i>	<i>a</i> <sup>0</sup> <i>a</i> <sup>0</sup> <i>c</i> <sup>-</sup>	No	NPD	(g)
Sr <sub>2</sub> FeNbO <sub>6</sub>	0.985	<i>I4/m</i>	<i>a</i> <sup>0</sup> <i>a</i> <sup>0</sup> <i>c</i> <sup>-</sup>	Yes	XRPD	(h)
Sr <sub>2</sub> FeTaO <sub>6</sub>	0.983	<i>Pnma</i>	<i>a</i> <sup>-</sup> <i>a</i> <sup>-</sup> <i>c</i> <sup>+</sup>	No	NPD	(i)
Ba <sub>2</sub> YNbO <sub>6</sub>	0.980	<i>Fm</i> $\bar{3}$ <i>m</i>	<i>a</i> <sup>0</sup> <i>a</i> <sup>0</sup> <i>a</i> <sup>0</sup>	Yes	NPD	(f)
Ca <sub>2</sub> AlNbO <sub>6</sub>	0.963	<i>P2</i> <sub>1</sub> / <i>n</i>	<i>a</i> <sup>-</sup> <i>a</i> <sup>-</sup> <i>c</i> <sup>+</sup>	Yes	XRPD	(j), (k), (f)
Sr <sub>2</sub> ScNbO <sub>6</sub>	0.963	<i>P2</i> <sub>1</sub> / <i>n</i>	<i>a</i> <sup>-</sup> <i>a</i> <sup>-</sup> <i>c</i> <sup>+</sup>	Yes	NPD	(f)
Ca <sub>2</sub> AlTaO <sub>6</sub>	0.963	<i>P2</i> <sub>1</sub> / <i>c</i> ‡	<i>a</i> <sup>-</sup> <i>a</i> <sup>-</sup> <i>c</i> <sup>+</sup>	Yes	XRPD	(l)
Sr <sub>2</sub> ScTaO <sub>6</sub>	0.961	<i>P2</i> <sub>1</sub> / <i>n</i>	<i>a</i> <sup>-</sup> <i>a</i> <sup>-</sup> <i>c</i> <sup>+</sup>	Yes	XRPD	(b)
Ca <sub>2</sub> CrNbO <sub>6</sub>	0.940	<i>P2</i> <sub>1</sub> / <i>n</i>	<i>a</i> <sup>-</sup> <i>a</i> <sup>-</sup> <i>c</i> <sup>+</sup>	Yes	XRPD	(m)
Ca <sub>2</sub> CrTaO <sub>6</sub>	0.937	<i>P2</i> <sub>1</sub> / <i>n</i>	<i>a</i> <sup>-</sup> <i>a</i> <sup>-</sup> <i>c</i> <sup>+</sup>	Yes	NPD	(b), (f)
Ca <sub>2</sub> GaTaO <sub>6</sub>	0.936	<i>P2</i> <sub>1</sub> / <i>n</i>	<i>a</i> <sup>-</sup> <i>a</i> <sup>-</sup> <i>c</i> <sup>+</sup>	Yes	XRPD	(b)
Sr <sub>2</sub> YbNbO <sub>6</sub>	0.933	<i>P2</i> <sub>1</sub> / <i>n</i>	<i>a</i> <sup>-</sup> <i>a</i> <sup>-</sup> <i>c</i> <sup>+</sup>	Yes	NPD	(n)
Ca <sub>2</sub> MnNbO <sub>6</sub>	0.931	<i>Pb</i> <i>n</i> <i>m</i> §	<i>a</i> <sup>-</sup> <i>a</i> <sup>-</sup> <i>c</i> <sup>+</sup>	No	XRPD	(g), (o)
Ca <sub>2</sub> FeNbO <sub>6</sub>	0.931	<i>P2</i> <sub>1</sub> / <i>n</i>	<i>a</i> <sup>-</sup> <i>a</i> <sup>-</sup> <i>c</i> <sup>+</sup>	Yes	XRPD	(g), (p)
Ca <sub>2</sub> FeTaO <sub>6</sub>	0.929	<i>P2</i> <sub>1</sub> / <i>n</i>	<i>a</i> <sup>-</sup> <i>a</i> <sup>-</sup> <i>c</i> <sup>+</sup>	Yes	XRPD	(b)
Ca <sub>2</sub> MnTaO <sub>6</sub>	0.929	<i>Pnma</i>	<i>a</i> <sup>-</sup> <i>a</i> <sup>-</sup> <i>c</i> <sup>+</sup>	No	XRPD	(b)
Sr <sub>2</sub> YNbO <sub>6</sub>	0.925	<i>P2</i> <sub>1</sub> / <i>n</i>	<i>a</i> <sup>-</sup> <i>a</i> <sup>-</sup> <i>c</i> <sup>+</sup>	Yes	NPD	(q)
Sr <sub>2</sub> YTaO <sub>6</sub>	0.923	<i>P2</i> <sub>1</sub> / <i>n</i>	<i>a</i> <sup>-</sup> <i>a</i> <sup>-</sup> <i>c</i> <sup>+</sup>	Yes	NPD	(q)
Ca <sub>2</sub> ScTaO <sub>6</sub>	0.909	<i>P2</i> <sub>1</sub> / <i>n</i>	<i>a</i> <sup>-</sup> <i>a</i> <sup>-</sup> <i>c</i> <sup>+</sup>	Yes	XRPD	(b)
Ca <sub>2</sub> YNbO <sub>6</sub>	0.874	<i>P2</i> <sub>1</sub> / <i>n</i>	<i>a</i> <sup>-</sup> <i>a</i> <sup>-</sup> <i>c</i> <sup>+</sup>	Yes	XRPD	(r)
Ca <sub>2</sub> YTaO <sub>6</sub>	0.873	<i>P2</i> <sub>1</sub> / <i>n</i>	<i>a</i> <sup>-</sup> <i>a</i> <sup>-</sup> <i>c</i> <sup>+</sup>	Yes	XRPD	(b)

References: (a) Tezuka *et al.* (2000); (b) Woodward (1997c); (c) Shan *et al.* (2001); (d) Woodward *et al.* (1994); (e) Yoshii (2000); (f) this work; (g) Lufaso *et al.* (2004); (h) Tao *et al.* (2004); (i) Cussen *et al.* (1997); (j) Vanderah *et al.* (2000); (k) Levin, Chan, Maslar, Vanderah & Bell (2001); (l) Sales *et al.* (1999); (m) Choy *et al.* (1996); (n) Yang *et al.* (1999); (o) Kruth *et al.* (1998); (p) Chakhmouradian & Mitchell (1998); (q) Howard *et al.* (2005); (r) Brusset *et al.* (1975). † Bond-valence parameter tolerance factors were calculated using *SPuDS*. ‡ *P2*<sub>1</sub>/*c* is the standard setting of *P2*<sub>1</sub>/*n*, but it is less convenient for describing perovskites. § *Pb**n**m* is a non-standard setting of *Pnma*.

larger studies of AMO<sub>3</sub> (Woodward, 1997b) and A<sub>2</sub>MM'O<sub>6</sub> perovskites (Lufaso *et al.*, 2006). The observation of cubic symmetry for Ba<sub>2</sub>YNbO<sub>6</sub> is perhaps unexpected for a compound with a tolerance factor as small as 0.98. This may suggest that when  $\tau$  is close to unity the structural preference (at room temperature) depends upon the characteristics of the A-site cation. Large polarizable cations like Ba<sup>2+</sup> may favor higher-symmetry structures, while small, harder cations like Ca<sup>2+</sup> may favor more distorted structures.

Perovskites are well known to be highly pseudosymmetric. When this effect becomes severe the structure determination process is complicated. The lack of reflection splitting can lead to an erroneous space-group assignment. The pathological peak overlap also tends to reduce the accuracy of the Rietveld refinements. Of the compounds whose structures are presented in this article, the three compounds where the A-site cation is Sr<sup>2+</sup> exhibit the most severe pseudosymmetry. This trend is not unique for these three compounds, as the unit-cell distortion indices, *D* (Arulraj *et al.*, 1998), given in Table 7, are very small for all compositions containing strontium on the A-site. It is tempting to think that the Ca<sup>2+</sup>-containing

compounds are less pseudosymmetric simply because the tolerance factor is smaller, which translates to more tilting and less pseudosymmetry. However, the results presented paint a more complicated picture. Consider the fact that Ca<sub>2</sub>AlNbO<sub>6</sub> and Sr<sub>2</sub>ScNbO<sub>6</sub> have tolerance factors that are essentially identical ( $\tau \simeq 0.96$ ), but the distortion of the unit-cell metrics of the two compounds are quite different. The Sr<sub>2</sub>ScNbO<sub>6</sub> diffraction data clearly shows that there is no reflection splitting out to 110° 2 $\theta$  and by all accounts this compound appears to have a metrically cubic unit cell (see Fig. 7). The unit-cell distortion parameter is only 0.07%, which is comparable to the pseudo-cubic tetragonal perovskites. It is only through the observation of extra reflections in the X-ray and neutron diffraction data that the monoclinic symmetry of this compound can be detected. In contrast, reflection splitting can clearly be seen in Ca<sub>2</sub>AlNbO<sub>6</sub> (see Fig. 7) and the unit-cell distortion parameter is much larger (*D* = 0.26%). Clearly, these differences cannot be explained solely on the basis of tolerance factor arguments, or even M–O–M' bond angles. The tendency for Sr<sub>2</sub>MM'O<sub>6</sub> compounds to possess more pseudo-

pseudosymmetry than Ca<sub>2</sub>MM'O<sub>6</sub> perovskites is considered in more detail in the following article (Lufaso *et al.*, 2006).

It is generally accepted that the extent of ordering in double perovskites is influenced by the differences in the charge and size of the octahedral-site cations (Anderson *et al.*, 1993), as well as bonding characteristics of the octahedral-site cations. Furthermore, the degree of long-range order is often kinetically limited and thus synthetic conditions can also play an important role (Woodward *et al.*, 1994). Within this context there are some interesting trends among the ordering characteristics of the compounds shown in Table 7. First, the observation of partial ordering in Sr<sub>2</sub>VTaO<sub>6</sub> shows that ordering can be achieved even when the octahedral cations have identical radii. Secondly, there does not appear to be a significant difference in the ordering characteristics of the niobates and the tantalates. Finally, while it is difficult to say from this limited sampling of compounds, it appears that there is a slight tendency for the long-range order to increase as the size of the A-site cation decreases (*i.e.* Ba<sub>2</sub>ScTaO<sub>6</sub> to Sr<sub>2</sub>ScTaO<sub>6</sub> to Ca<sub>2</sub>ScTaO<sub>6</sub>). This latter factor may be due to changes in the melting point that influence diffusion rates at

the synthesis temperature. In some compounds there is a tendency for the  $\text{Ca}^{2+}$  ion to disorder slightly with the  $M^{3+}$  ion, thereby increasing the size and charge difference with respect to the  $M^{5+}$  cation. This effect is observed for  $\text{Ca}_2\text{YNbO}_6$ .

## 5. Conclusions

The crystal structures of six  $A_2MTaO_6$  and  $A_2MNbO_6$  perovskites have been determined through analysis of neutron

powder diffraction data using a systematic approach to avoid erroneous assignments that can arise from pseudosymmetry. Additionally, space-group assignments, cation ordering and unit-cell dimensions are presented for an additional 13 ordered perovskites from analysis of synchrotron and monochromatic laboratory X-ray data. Pseudosymmetry in perovskites is exceptionally pronounced in compositions where  $A = \text{Sr}^{2+}$ . The origin of this effect is not well understood, but it makes structure determination for these compounds significantly

more difficult. These studies taken together with previous works reveal a strong correlation between the tolerance factor and the space-group symmetry. Reports of compounds with cubic symmetry having tolerance factors less than 1 should be viewed with caution, in the absence of a careful NPD analysis. In the case of  $\text{Sr}_2\text{GaTaO}_6$  and  $\text{Sr}_2\text{CrTaO}_6$  the strong pseudosymmetry makes it very difficult to distinguish between tetragonal  $a^0a^0c^-$  ( $I4/m$ ) and cubic  $a^0a^0a^0$  ( $Fm\bar{3}m$ ) structures. The assignment of tetragonal symmetry can only be made through comparison of the intensities of the  $R$ -point superlattice reflections. In the case of  $\text{Sr}_2\text{ScNbO}_6$  the pseudosymmetry is so severe that the unit-cell dimensions are effectively cubic, yet the crystallographic symmetry is monoclinic. Since the X-ray scattering power of oxygen is small compared with many cations, neutron data is vital for conclusively determining the structures of these compounds.

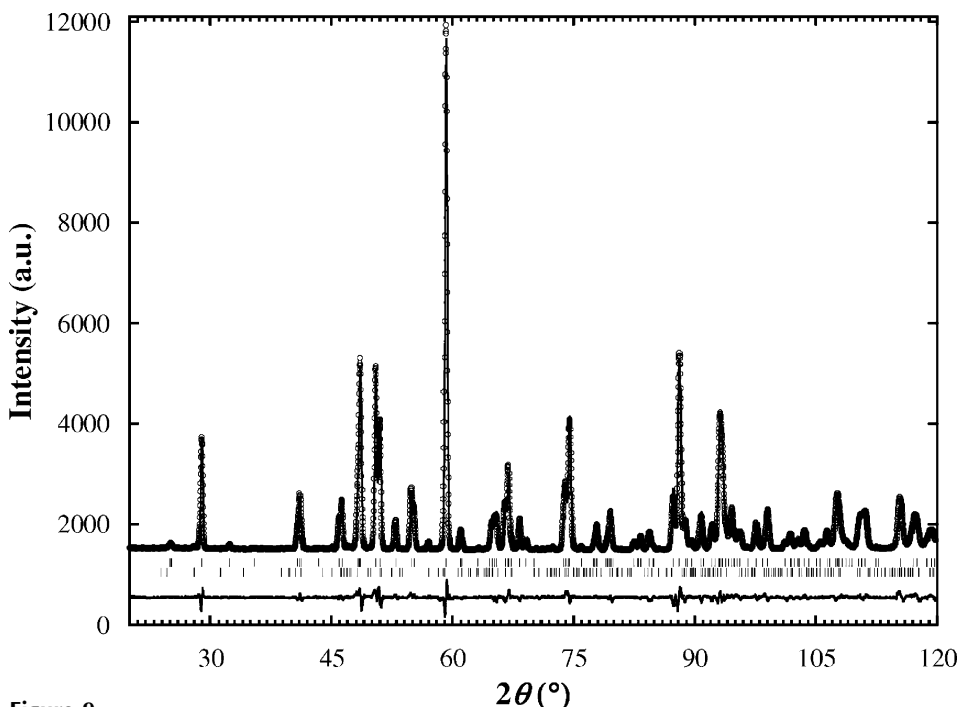


**Figure 9** Observed neutron diffraction pattern along with calculated and difference patterns from the Rietveld refinement of  $\text{Ca}_2\text{CrTaO}_6$ . The second set of reflection position markers are for the impurity phase  $\text{Ca}_3(\text{CaTa}_2)\text{O}_9$ . The structure model for the impurity phase is based on the structure of  $\text{Ca}_3(\text{CaNb}_2)\text{O}_9$  (Levin, Chan, Geyer, Maslar & Vanderah, 2001). Vertical bars shown between the fit data and difference patterns indicate the  $2\theta$  position of the observed reflections.

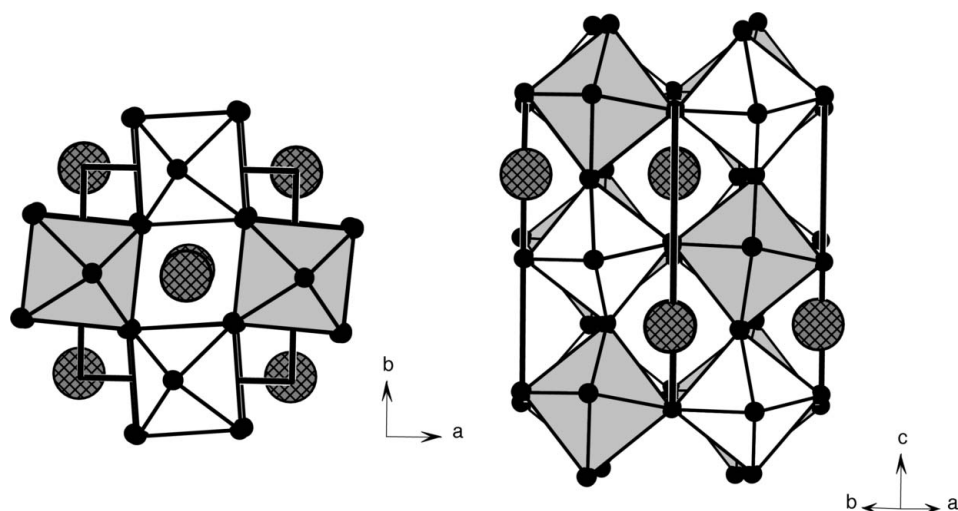


**Figure 10** The structure of  $\text{Sr}_2\text{ScNbO}_6$  (space group  $P2_1/n$ ; tilt system:  $a^-a^-c^+$ ). Both in-phase and out-of-phase tilting occurs in observed. Legend:  $[\text{ScO}_6]$ : white octahedra;  $[\text{NbO}_6]$ : grey octahedra; Sr: cross-hatched spheres; O: filled spheres.

Research carried out in part at the National Synchrotron Light Source at Brookhaven National Laboratory is supported by the US Department of Energy (Contract No. DE-AC02-98CH10886 for beamline X7A). We acknowledge the support of the National Institute of Standards and Technology, US Department of Commerce, in providing the neutron research facilities used in this work. The authors acknowledge the National Science Foundation supported Center for the Design of Materials (CHE-043567) and The Ohio State University for financial support. A.

W. Sleight is acknowledged for the initial inspiration for this work and many valuable discussions. We would also like to acknowledge T. Vogt for collection of the BNL neutron data, and H. W. Eng and M. Avdeev for numerous discussions.

## References

- Aleksandrov, K. S. (1976). *Sov. Phys. Crystallogr.* **21**, 133.
- Aleksandrov, K. S. & Misyul, S. V. (1981). *Sov. Phys. Crystallogr.* **26**, 612–618.
- Alonso, J. A., Martinez-Lope, M. J., Casais, M. T. & Fernandez-Diaz, M. T. (2000). *Inorg. Chem.* **39**, 917–923.
- Anderson, M. T., Greenwood, K. B., Taylor, G. A., Poepfelmeier, K. R. (1993). *Prog. Solid State Chem.* **22**, 197–235.
- Arulraj, A., Biswas, A., Raychaudhuri, A. K., Rao, C. N. R., Woodward, P. M., Vogt, T., Cox, D. E. & Cheetham, A. K. (1998). *Phys. Rev. B*, **57**, R8115.
- Balić Žunić, T. & Makovicky, E. (1996). *Acta Cryst.* **B52**, 78–81.
- Barnes, P. W. (2003). PhD Dissertation. The Ohio State University, Columbus, Ohio, USA.
- Bieringer, M., Moussa, S. M., Noailles, L. D., Burrows, A., Kiely, C. J., Rosseinsky, M. J. & Ibberson, R. M. (2003). *Chem. Mater.* **15**, 586–597.
- Bock, O. & Müller, U. (2002). *Acta Cryst.* **B58**, 594–606.
- Brandle, C. D. & Fratello, V. J. (1990). *J. Mater. Res.* **5**, 2160–2164.
- Brixner, L. (1960). *J. Inorg. Nucl. Chem.* **15**, 352–355.
- Brown, I. D. & Altermatt, D. (1985). *Acta Cryst.* **B41**, 244–247.
- Brusset, H., Gillier-Pandraud, H. & Rajaonera, P. (1975). *Mater. Res. Bull.* **10**, 209–216.
- Chakhmouradian, A. R. & Mitchell, R. H. (1998). *J. Solid State Chem.* **138**, 272–277.
- Choy, J.-H., Hong, S.-T. & Choi, K.-S. (1996). *J. Chem. Soc. Faraday Trans.* **92**, 1051–1059.
- Choy, J.-H., Park, J.-H., Hong, S.-T. & Kim, D.-K. (1994). *J. Solid State Chem.* **111**, 370–379.
- Cussen, E. J., Vente, J. F., Battle, P. D. & Gibb, T. C. (1997). *J. Mater. Chem.* **7**, 459–463.
- Darlington, C. N. W. (2002). *Acta Cryst.* **A58**, 66–71.
- Davies, P. K. (1999). *Curr. Opin. Solid State Mater. Sci.* **4**, 467–471.
- Evdokimov, A. A. & Men'shenina, N. F. (1982). *Z. Neorg. Khim.* **27**, 2137–2139.
- Filip'ev, V. S. & Fesenko, E. G. (1961). *Kristallografiya*, **6**, 770–772.
- Filip'ev, V. S. & Fesenko, E. G. (1966). *Sov. Phys. Crystallogr.* **10**, 243–247.
- Glazer, A. M. (1972). *Acta Cryst.* **B28**, 3384–3392.
- Glazer, A. M. (1975). *Acta Cryst.* **A31**, 756–762.
- Goldschmidt, V. M. (1926). *Naturwissenschaften*, **14**, 477–485.
- Henmi, K., Hinatsu, Y. & Masaki, N. M. (1999). *J. Solid State Chem.* **148**, 353–360.
- Howard, C. J., Barnes, P. W., Kennedy, B. J. & Woodward, P. M. (2005). *Acta Cryst.* **B61**, 258–262.
- Howard, C. J., Kennedy, B. J. & Woodward, P. M. (2003). *Acta Cryst.* **B59**, 463–471.
- Howard, C. J. & Stokes, H. T. (1998). *Acta Cryst.* **B54**, 782–789.
- Howard, C. J. & Stokes, H. T. (2002). *Acta Cryst.* **B58**, 565.
- Howard, C. J. & Stokes, H. T. (2004). *Acta Cryst.* **B60**, 674.
- Howard, C. J. & Stokes, H. T. (2005). *Acta Cryst.* **A61**, 93–111.
- Kobayashi, K. L., Kimura, T., Sawada, H., Terakura, K. & Tokura, Y. (1998). *Nature*, **395**, 677–680.
- Kruth, A., Tabuchi, M., Guth, U. & West, A. R. (1998). *J. Mater. Chem.* **8**, 2515–2520.
- Laron, A. C. & von Dreele, R. B. (2000). GSAS. Report LAUR 86–748. Los Alamos National Laboratory, Los Alamos, New Mexico, USA.
- Levin, I., Chan, J. Y., Geyer, R. G., Maslar, J. E. & Vanderah, T. A. (2001). *J. Solid State Chem.* **156**, 122–134.
- Levin, I., Chan, J. Y., Maslar, J. E., Vanderah, T. A. & Bell, S. M. (2001). *J. Appl. Phys.* **90**, 904–914.
- Lufaso, M. W., Barnes, P. W. & Woodward, P. M. (2006). *Acta Cryst.* **B62**, 397–410.
- Lufaso, M. W. & Woodward, P. M. (2001). *Acta Cryst.* **B57**, 725–738.
- Lufaso, M. W., Woodward, P. M. & Goldberger, J. E. (2004). *J. Solid State Chem.* **177**, 1651–1659.
- Mitchell, R. H. (2002). *Perovskites Modern and Ancient*. Thunder Bay, MI: Almaz Press.
- Rodríguez-Carvajal, J. (1993). *Physica B*, **192**, 55–59.
- Roissnel, T. & Rodríguez-Carvajal, J. (2001). *Mater. Sci. Forum*, Proc. of the European Powder Diffraction Conference (EPDIC), Barcelona May 2000, Vol. 378–381, pp. 118–123.
- Sales, M., Eguia, G., Quintana, P., Torres-Martinez, L. M. & West, A. R. (1999). *J. Solid State Chem.* **143**, 62–68.
- Shan, Y. J., Ozeki, A., Luan, W., Nakamura, T. & Itoh, M. (2001). *Ferroelectrics*, **264**, 175–180.
- Sleight, A. W. (1963). PhD Dissertation, University of Connecticut, USA.
- Sleight, A. W. & Weiher, J. F. (1972). *J. Phys. Chem. Solids*, **33**, 679–687.
- Tao, S., Canales-Vazquez, J. & Irvine, J. T. S. (2004). *Chem. Mater.* **16**, 2309–2316.
- Tezuka, K., Henmi, K., Hinatsu, Y. & Masaki, N. M. (2000). *J. Solid State Chem.* **154**, 591–597.
- Thomas, N. W. (1989). *Acta Cryst.* **B45**, 337–344.
- Thomas, N. W. (1996a). *Acta Cryst.* **B52**, 16–31.
- Thomas, N. W. (1996b). *Acta Cryst.* **B52**, 954–960.
- Toby, B. H. (2001). *J. Appl. Cryst.* **34**, 210–213.
- Vanderah, T. A. (2002). *Science*, **298**, 1182–1184.
- Vanderah, T. A., Febo, W., Chan, J. Y., Roth, R. S., Loezos, J. M., Rotter, L. D., Geyer, R. G. & Minor, D. B. (2000). *J. Solid State Chem.* **155**, 78–85.
- Woodward, P. M. (1997a). *Acta Cryst.* **B53**, 32–43.
- Woodward, P. M. (1997b). *Acta Cryst.* **B53**, 44–66.
- Woodward, P. M. (1997c). PhD Dissertation. Oregon State University, Corvallis, Oregon, USA.
- Woodward, P., Hoffmann, R. D. & Sleight, A. W. (1994). *J. Mater. Res.* **9**, 2118–2127.
- Yang, J. H., Choo, W. K., Lee, J. H. & Lee, C. H. (1999). *Acta Cryst.* **B55**, 348–354.
- Yoshii, K. (2000). *J. Alloys Compd.* **307**, 119–123.